This is to certify that the

thesis entitled

Teleseismic Mislocations of Earthquakes in
Island Arcs - Theoretical Results

presented by

Timothy Lynn Nieman

has been accepted towards fulfillment
of the requirements for

M.S. degree in Geological Sciences

Kazuya Fujita
Major professor
Kazuya Fujita

Date May 2, 1985

O-7639

# TELESEISMIC MISLOCATION OF EARTHQUAKES IN ISLAND ARCS - THEORETICAL RESULTS

By

Timothy Lynn Nieman

A THESIS

Submitted to
Michigan State University
in partial fulfillment of the requirements
for the degree of

MASTER OF SCIENCE

Department of Geological Sciences

1985

3346705

## ABSTRACT


TELESEISMIC MISLOCATIONS OF EARTHQUAKES
IN ISLAND ARCS - THEORETICAL RESULTS

By

Timothy Lynn Nieman

Three-dimensional seismic ray tracing through thermally derived slab models is used to investigate the effects of subducting lithosphere on teleseismic earthquake locations in island arcs. Theoretical results show teleseismic mislocations are greatest in the thrust zone and become negligible seaward of the trench. Varying the thermal coefficient and depth of penetration of the model slab have pronounced effects on mislocations while variations in assumed slab thickness have only minor effects. Variations in station distributions used to locate island arc events can result in 10 km difference in determined epicenters for the same event.

Comparison with observed mislocations gives a best fit model for the central Aleutian slab extending to 360 km depth with a thermal coefficient of -.0009 km/sec-°C. Theoretical mislocations indicate that intermediate depth events are well located teleseismically. Spurious slab dips and thinning of the Benioff zone can result from mislocations of deeper events.

## ACKNOWLEDGMENTS

I would like to thank my advisor and committee chairman, Kazuya Fujita, for this thesis topic, for keeping my computer account loaded, and for numerous forms of aid, encouragement, and criticism. Thanks also go to Fate, for not presenting the opportunity for Kaz to shove raw fish down my throat. I would like also to thank the other members of my committee, Hugh F. Bennett and F. William Cambray, for their help and criticism. Special thanks to Mom and Dad, whose encouragement, understanding, and money helped make this possible, and to the Copper's for much needed breaks at their desert resort complex. I am grateful to my friends and colleagues, Don, Dave, Cindy, Bruce, Soo Meen, Bill, and Greg, and, of course, the entire cast of Geo Inc in its various forms, for their friendship and help in attitude adjustment when needed. Thanks to the faculty and staff at Michigan State University for their support and cooperation.

This research was supported, in part, by NSF grant EAR 80-25267. The author was supported by a Chevron Graduate Fellowship and the Department of Geological Sciences at Michigan State University.

TABLE OF CONTENTS

# LIST OF TABLES

## LIST OF FIGURES

# INTRODUCTION

Analyses of locations of earthquakes and nuclear explosions in island arc regions show that velocity inhomogeneities due to subducting lithospheric slabs can induce location errors of 50 km or more (Herrin and Taggert,1968; Utsu, 1971; Engdahl,1977), for teleseismically located island arc earthquakes, when standard symmetric earth location procedures are used. Higher seismic velocities within the slab, as compared with the adjacent mantle, can result in P-wave travel time advances in excess of 5 seconds (Jacob,1970; Sleep,1973) as well as shadow zones caused by refraction through the slab (Sleep,1973). Clearly, understanding the geometry and rheological properties of descending lithosphere is intimately related to being able to accurately locate earthquakes occurring there. In recent years, data from local seismic networks has greatly improved our understanding of subducting slabs and their effects on ray paths (Engdahl et al.,1977b; Hasegawa et al.,1978; Fujita et al., 1981; Frohlich et al.,1982).

Numerous studies have been performed to delineate slab structure by looking at how the high-velocity subducting lithosphere affects travel times (Sleep, 1973; Hasegawa et al., 1978; Fujita et al., 1981; Frohlich et al.,1982; Spencer and Engdahl, 1983; Mclaren and Frohlich,1985). Ideally, the most precise approach involves the use of three-dimensional seismic ray tracing through realistic, detailed velocity structures. However, computational inefficiency in tracing rays from a source to a large number of stations generally makes the side by side comparison of numerous models impractical. Fujita et al. (1981) developed a method that achieves a significant reduction in computation time required. Instead of trying to home a ray into each individual station, they shoot a variable coverage of the focal sphere and interpolate to find travel times to individual stations. They also noted that unless the slab is torn or contorted, its effects on locations are a smooth function of epicentral distance from the center of arc curvature for any constant given focal depth. It is therefore only necessary to determine the slab's effects at various evenly spaced points and interpolate for effects at intermediate points. In this study, I use this approach to investigate and clearly demonstrate the mislocation effects of a fairly large number of models for the subducting slab in the central Aleutian Islands, Alaska.

I also compare modeled mislocations with mislocations of actual earthquakes in an effort to constrain several physical properties of the subducting slab. Estimates of errors in ISC (International Seismological Centre) and PDE (Preliminary Determination of Epicenters) reported teleseismic hypocentral solutions can be made by comparison with locations determined from only local network data. This study concerns the area near Adak Island, where a local seismic network has been in operation since late July, 1974. Local epicentral solutions for shallow thrust zone events near Adak are believed to be accurate to within a few kilometers (Frohlich et al.,1982).

# METHODOLOGY

The method of model generation, ray tracing, and relocation is basically the same as that of Fujita et al. (1981) with several minor changes. Essentially the procedure is as follows. Thermal modeling was used to determine velocity structure for various combinations of three parameters; slab thickness, depth of slab penetration, and thermal coefficient of seismic velocity. Seismic ray tracing was performed through the models to obtain P-wave travel time anomalies from hypothetical earthquakes to a network of stations. Computed travel times were then used to relocate the theoretical events using a standard symmetric earth location routine. The original hypocenter was compared with the relocated hypocenter in order to determine the mislocation vector for a given theoretical earthquake and slab model. Mislocation vectors for actual earthquakes could then be compared with model mislocation vectors to evaluate the feasibility of the specific model.

The finite difference modeling technique of Toksoz et al. (1971,1973) was used to produce temperature profiles for each model. Using the Herrin et al. (1968) velocities as the base model, velocity profiles were constructed from the thermal profiles using a linear relation between velocity and temperature anomaly. Laboratory experiments give values for this thermal coefficient ($\partial v/\partial T$ in eq. 1: Sleep, 1973) around $-5 \times 10^{-4}$ km/sec-°C (Anderson et al.,1968), while many authors have reasoned that realistic earth values are greater in magnitude (Sleep,1973;Engdahl et al.,1977b; Fujita et al.,1981; also Jacob, 1972; Hasegawa et al., 1978 based on velocity contrast considerations). I allowed the thermal coefficient to vary from $-5 \times 10^{-4}$ to an assumed maximum of $-9 \times 10^{-4}$ km/sec-°C in an attempt to constrain its value.

Three dimensional velocity representations were constructed by rotating the two dimensional model about the center of curvature of the island arc located at 63.314°N and 178.059°W (Engdahl, 1977; Fujita et al.,1981). Positions on a cross section of the subduction zone can then be described simply in terms of depth and distance ($\partial$) from the pole. This places the volcanic arc at 11.4° $\partial$ (distance from center of arc curvature) and the trench axis at 13.0° $\partial$ for the Adak region. A diagram of the model slab is shown in Figure 1.

I followed Fujita et al.'s (1981) scheme for ray tracing, plotting, and digitizing exactly except that I digitized every 5° of azimuth instead of

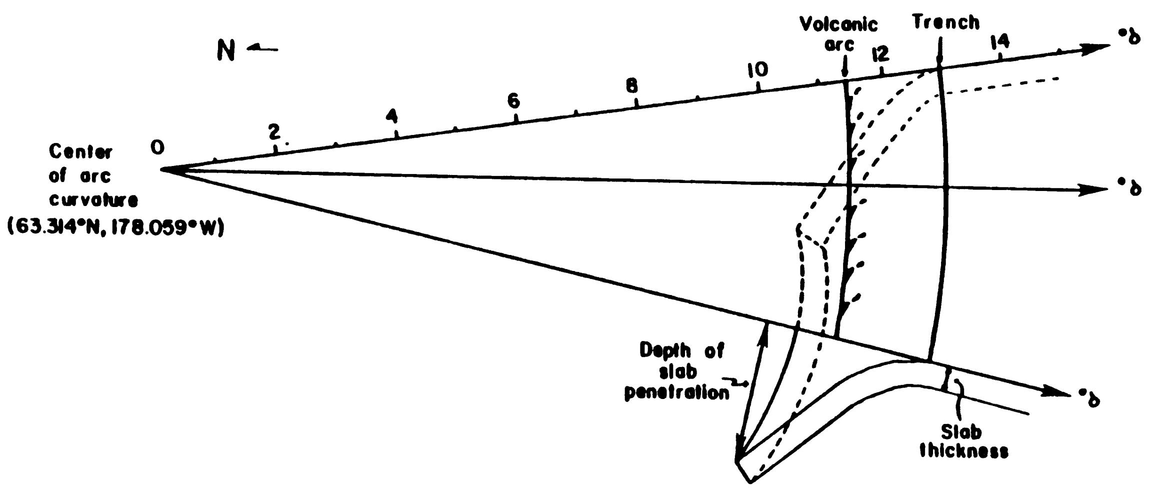


Figure 1. Model Slab Parameters.
Diagram showing how model slab is represented three-dimensionally.
δ is the geocentric distance in degrees from the center of arc curvature.

every 10°, and I used 13 Fourier coefficients instead of 9. These improvements in accuracy were needed since I examined models having more pronounced azimuthal variations of residuals.

Relocations of the hypothetical earthquakes were performed using two different station sets, each consisting of stations between 30° and 90° geocentric distance, with the addition of local station ADK for depth and origin time control. Travel times were determined by applying interpolated residuals to a modified Herrin travel time table. In an effort to obtain more realistic travel times to ADK, Herrin travel times for distances of less than 5° were adjusted to reflect the local ADK shallow velocity structure (Toth and Kisslinger, 1984), assuming that this structure is representative of both source and receiver velocities. Standard Herrin travel times were used for teleseismic distances.

The existence of a strong azimuthal bias in travel time residuals necessitated the consideration of station distributions used to locate different earthquakes. For the central Aleutians, smaller magnitude events are generally recorded best in western North America and moderately well in northern Europe while larger events are very well recorded in Europe and southern Asia as well as North America. Relocations of hypothetical events indicate epicentral differences of up to 10 km can occur for the same event when located using two different station sets, one set typical of smaller central Aleutian events (~4.7 Mb) and one typical of larger events (~5.4 Mb). Ideally, for each actual earthquake used to compare with model earthquakes, I would like to have performed theoretical event relocations using the same station set reporting the actual event, but time and cost limitations made this impractical. Therefore, station geometries for approximately 50 thrust zone events were examined to determine an "average" station set. It was noted that the distribution of stations reporting arrivals is more dependent on the number of stations reporting than on listed body wave magnitudes, with a general change in geometric distribution occurring at about 175 reporting stations. I thus compiled two station sets using the most commonly reporting stations for the events examined. One station set consisting of 220 stations was used to represent an "average" station distribution for larger earthquakes (events reported by more than 175 total stations) while the other, consisting of 110 stations, was used to represent smaller events (reported by 50 to 175 total stations).

Earthquakes to be used as the data base with which to compare model mislocations had to be well recorded both teleseismically and locally. For the time span of August, 1974 through February, 1979 and January, 1982 through October, 1983, I compiled an initial list of 40 shallow (<50 km depth) events between 175°W and 179°W recorded by the local network (Engdahl et al., 1977a; Engdahl et al., 1982; Kisslinger et al., 1982; Kisslinger et al., 1984) and by at least 50 total stations in the ISC or PDE bulletins. In order to be consistent with the hypothetical event location method, the actual events were relocated using Herrin travel times and only stations at distances of 30° to 90° ,plus ADK. Stations with spurious travel times (residual > 3 sec) were discarded. Relocations were done both with and without station corrections (Dziewonski and Anderson, 1983) with an average location difference of 2.7 km in epicenter and 2.9 km in depth between the two methods for the 40 events used in this study. Generally, smaller events (50 to 100 stations) showed the greatest location changes when station corrections were used, with a maximum epicentral change of 10.4 km in the Feb 18,1976 event. The average RMS residual for the locations was reduced from .823 to .778 seconds when corrections were used. The hypocenters determined with station corrections were used as the data set.

## MISLOCATION RESULTS

Most previous studies employing thermal modeling and ray tracing for the central Aleutians have assumed slabs which penetrate no deeper than 300 km. Sleep (1973) used a slab extending to 180 km depth with $\partial v/\partial T$ = $-9 \times 10^{-4}$ km/sec-°C for the region near Amchitka Island, approximately 200 km west of Adak Island. One would expect the slab to penetrate to a shallower depth at Amchitka than at Adak since subduction becomes more oblique as one moves west along the Aleutian arc. A number of recent studies of the Adak region have used a slab which is 80 km thick, penetrates to a depth of 300 km, and also with a thermal coefficient of $-9 \times 10^{-4}$ (Fujita et al., 1981; Engdahl et al., 1982; Rogers, 1982). Figure 2 shows the velocity profile for this model, which gives an average velocity contrast of ~6% and a maximum velocity contrast of ~10% compared with the ambient mantle. I chose this as the first model for study. Assuming this model is essentially correct, I performed theoretical relocations to determine the mislocations that should be observed for events in this area.

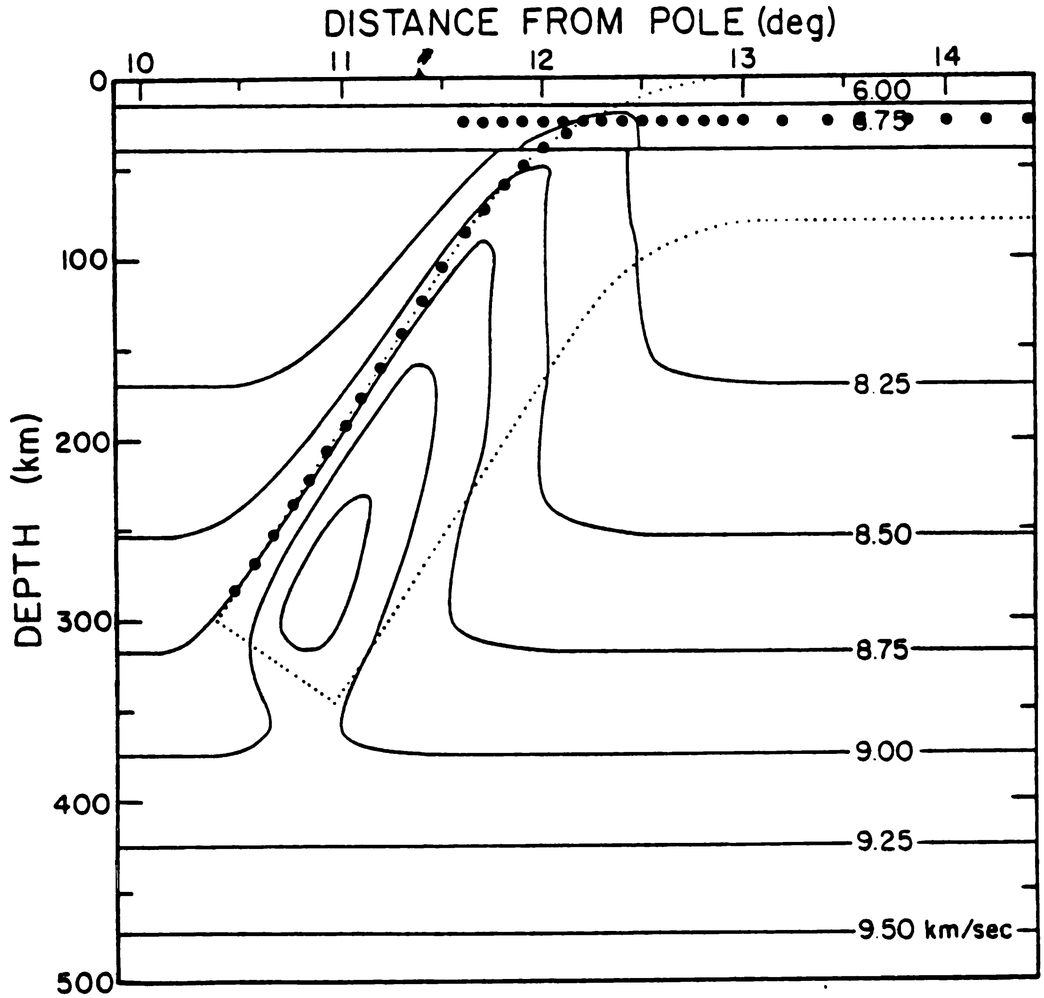


Figure 2. Velocity Profile of 300 x 80, -.0009 Slab. Triangle at a distance 11.4° at the surface indicates location of volcanic front. Solid dots indicate locations of theoretical events for this model. Slab is outlined by dotted line. (from Fujita et al., 1981)

Shallow Events

Ray tracing and relocations were computed for theoretical earthquakes located every 0.1° from 11.6° to 13.0° ∂ and every 0.2° from 13.2° to 14.6° ∂ at a depth of 25 km. The left sides of the plots in Figure 3 show two of the contoured residual maps from ray tracing for events located at 12.0° ∂ and 12.4° ∂. For these events, the greatest travel time advances occur at an azimuth of ~60° and ~55°, respectively. In general, rays traveling laterally down dip, as opposed to directly down dip, travel the greatest distance within the slab and thus result in the greatest residuals. As the geometry of the situation would predict, the region of greatest residuals rotates toward 0° azimuth with increasing ∂. The right sides of the plots show emergence points for equal takeoff azimuths (solid lines) and equal takeoff angles (dotted lines or solid dots).

Figures 4 and 5 show plots of mislocation vectors for shallow events in this model done with the two station sets, open circles indicating original locations and solid circles showing hypocenters upon relocation. Figures 4 and 5 verify the assumption that mislocations are a smooth function of ∂ (Fujita et al., 1981). Therefore, in order to save time and expense, all subsequent models were done with a wider spacing of theoretical events

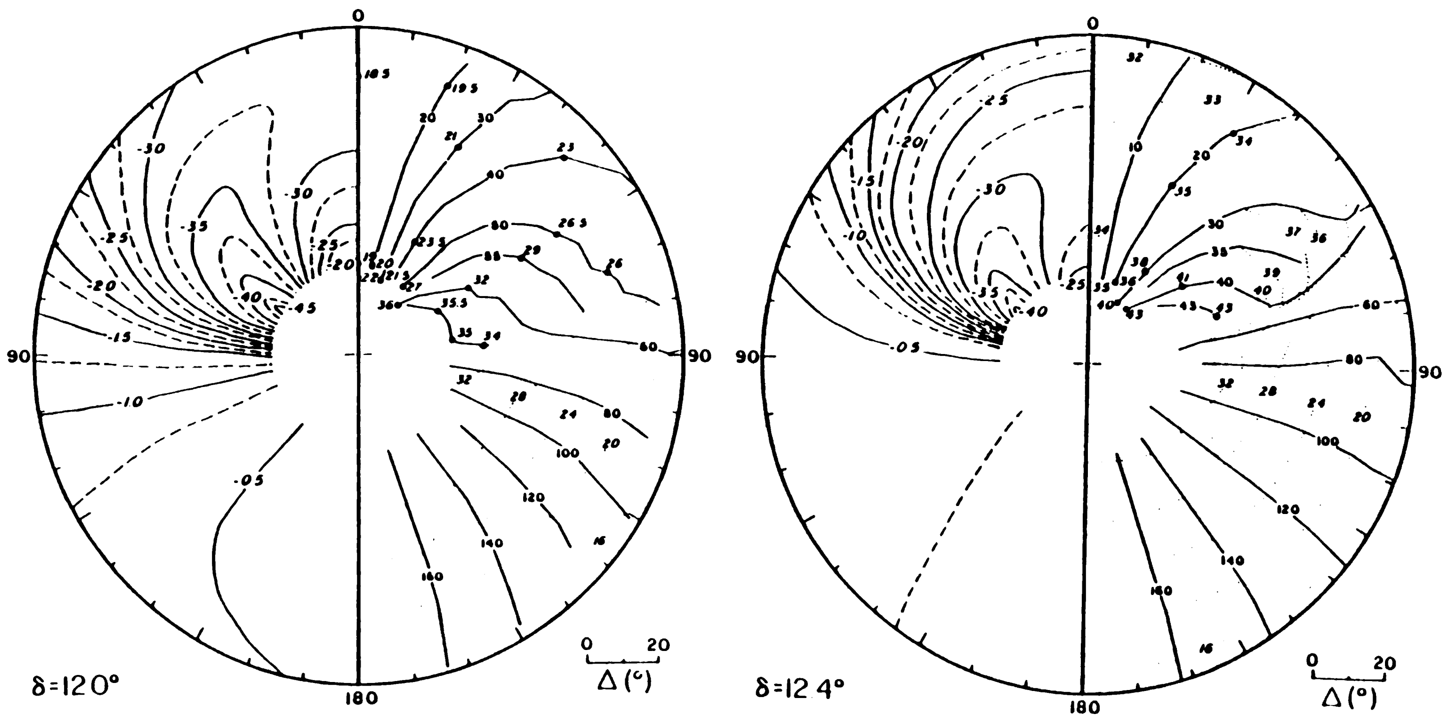


Figure 3. Travel-time Residuals.
Travel-time residuals calculated by seismic ray tracing through a 300 km deep by 80 km thick slab with a thermal coefficient of -.0009 km/sec-°C are contoured at 0.25 second intervals and plotted on the left half of an equidistant azimuthal projection about 25 km focal depth hypocenters at δ=12.0° (left) and δ=12.4° (right). Calculated initial ray parameters for emergence points are plotted on the right half; initial take-off angles in degrees are shown by dotted lines at 4° intervals or as solid dots; initial take-off azimuths are shown by solid lines at 10° or 20° intervals. Supplemental take-off azimuths and angles are shown where needed. (from Fujita et al., 1981)

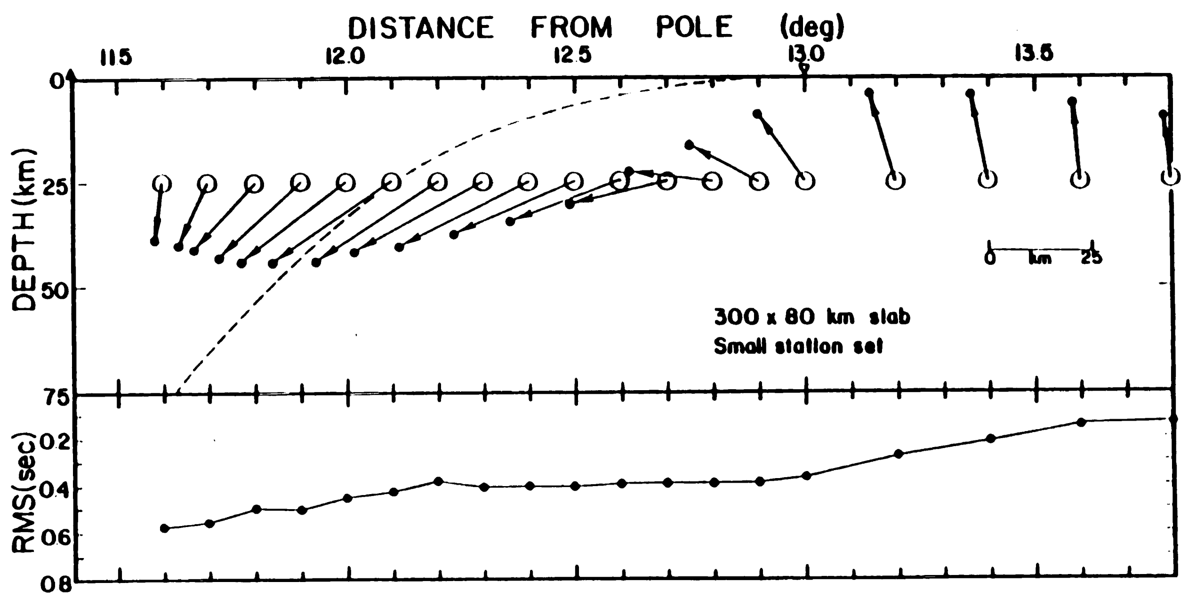


Figure 4. Shallow Event Mislocation Vectors for 300 x 80 km, -.0009 Slab, Small Station Set. Open circles represent original locations of hypothetical events. Solid dots represent hypocenters upon relocation. Solid triangle and open triangle represent volcanic front and trench, respectively. Dashed line represents upper surface of slab. RMS residuals for relocations are shown in bottom part of figure.

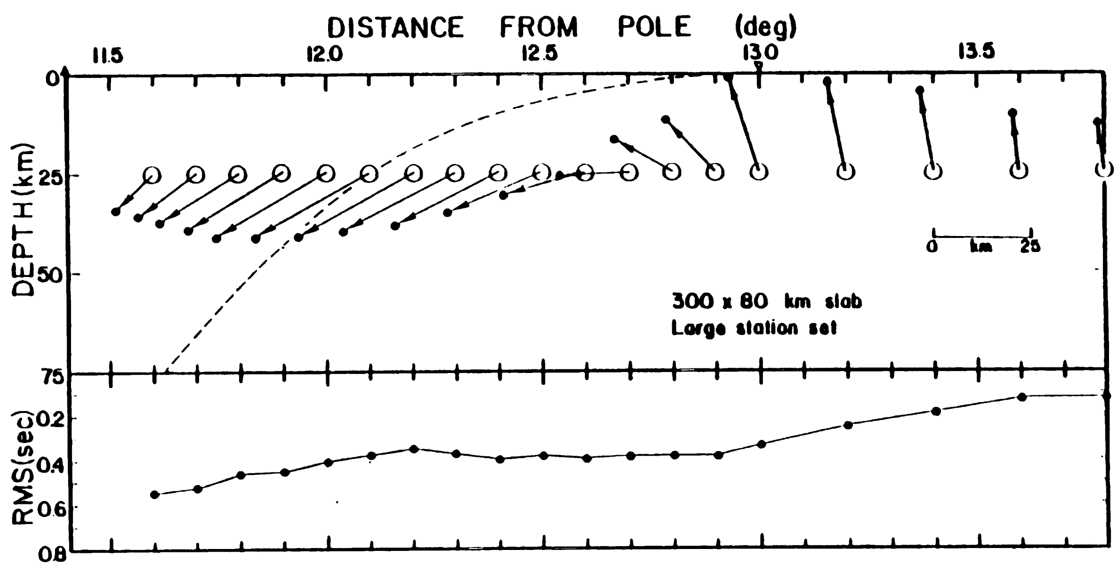


Figure 5. Shallow Event Mislocation Vectors for 300 x 80 km, -.0009 Slab, Large Station Set. Symbols same as in Figure 4.

with interpolation used between events. For this model (and, as will be shown, for all models in this study), mislocations are greatest in the thrust zone near 12.2° ∂. Also seen is that epicentral mislocations become negligible, given the limits of location procedures, seaward of the trench. The mislocation vectors suggest that events may actually be located too shallowly near to and seaward of the trench.

## Effects of Station Geometry

Figure 6 shows only epicentral mislocations as a function of ∂ for relocations done with the two different station sets. Mislocations are greater for locations done with the large station set on the volcanic arc side of the thrust zone. Mislocations are about equal at 12.1° ∂; seaward of this point, mislocations are greater when the smaller station set is used. One reason for this pattern can be seen by considering the station sets (Figure 7) and the residual patterns (Figure 3). The major difference in coverage between the two station sets occurs in Europe and southern Asia between about 76° and 90° geocentric distance from 320° and 360° azimuth, with the large station set showing a significantly better coverage of this area. Travel time residuals are up to one second greater in this area for a ∂ of 12.0° than for 12.4°, hence the greater mislocations. This

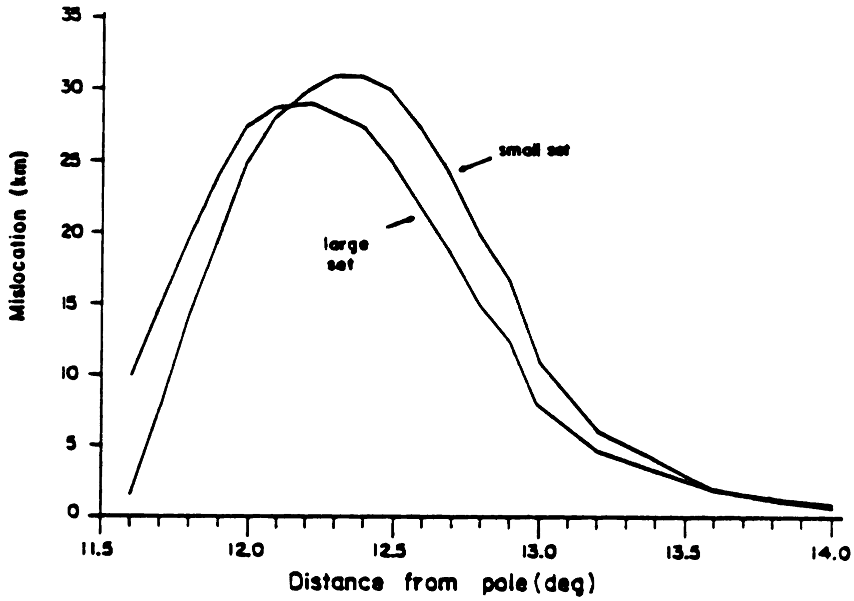


Figure 6. Epicentral Mislocations for Different Station Sets. Comparison of epicentral mislocations using station sets representative of "small" and "large" events near Adak for 300 x 80 km model with a thermal coefficient of -.0009 km/sec-°C.

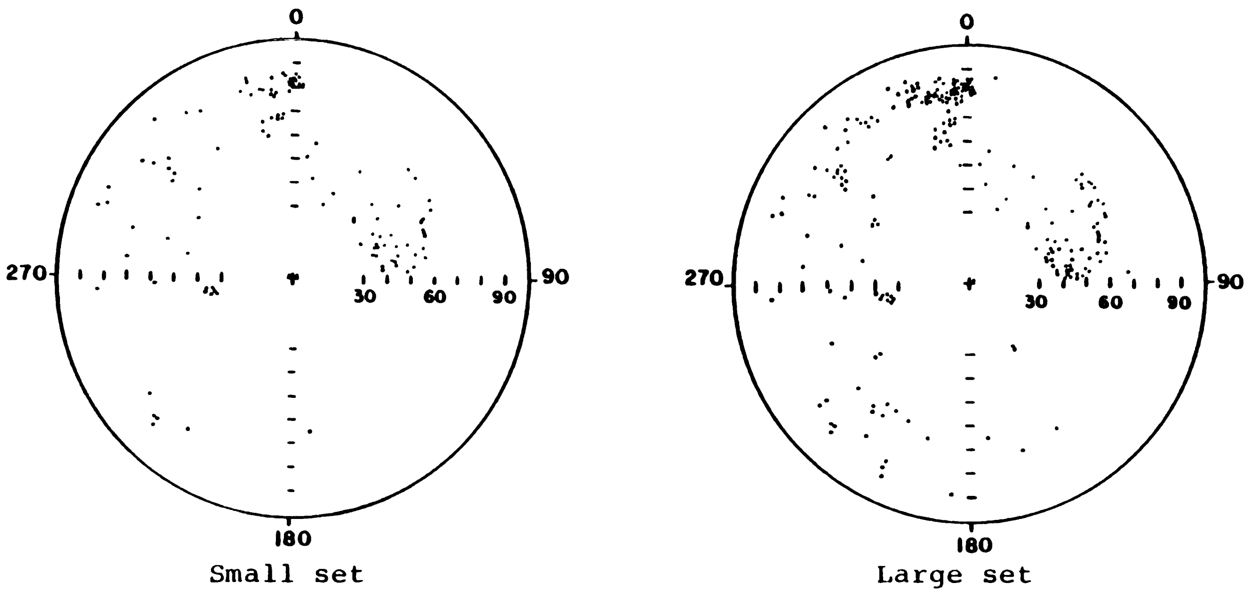


Figure 7. Station Distributions.
Equidistant azimuthal plots of stations used to relocate hypothetical events. Center of plots is located in the thrust zone 12.2° from the center of arc curvature (51.114°N, 178.059°W).

general pattern (Figure 6) holds for all models used in this study; as the length of the model slab increases, though, the point where the mislocations are equal for both station sets shifts slightly towards smaller $\partial$'s.

## Deeper Events

For this model (and for one other model which will be discussed later) I also performed ray tracing and relocations for a series of theoretical events located at depth along the upper surface of the descending slab. The degree of mislocation for deeper events proved to be relatively insensitive to which station set was used. The probable reason for this is that rays traveling from deep events to European stations, where the major difference in the station set coverages exists, are largely unaffected by the slab. All deep event teleseismic relocations shown in this study are done with the large station set. The results are basically the same if the relocations are done with the small station set.

Figure 8 shows the mislocation vectors, which predict that teleseismic mislocations for events deeper than about 100 km are small (always less than 10 km) supporting previous findings (Barazangi and Isacks, 1979; Engdahl et al., 1982) which suggest that teleseismic locations of deep

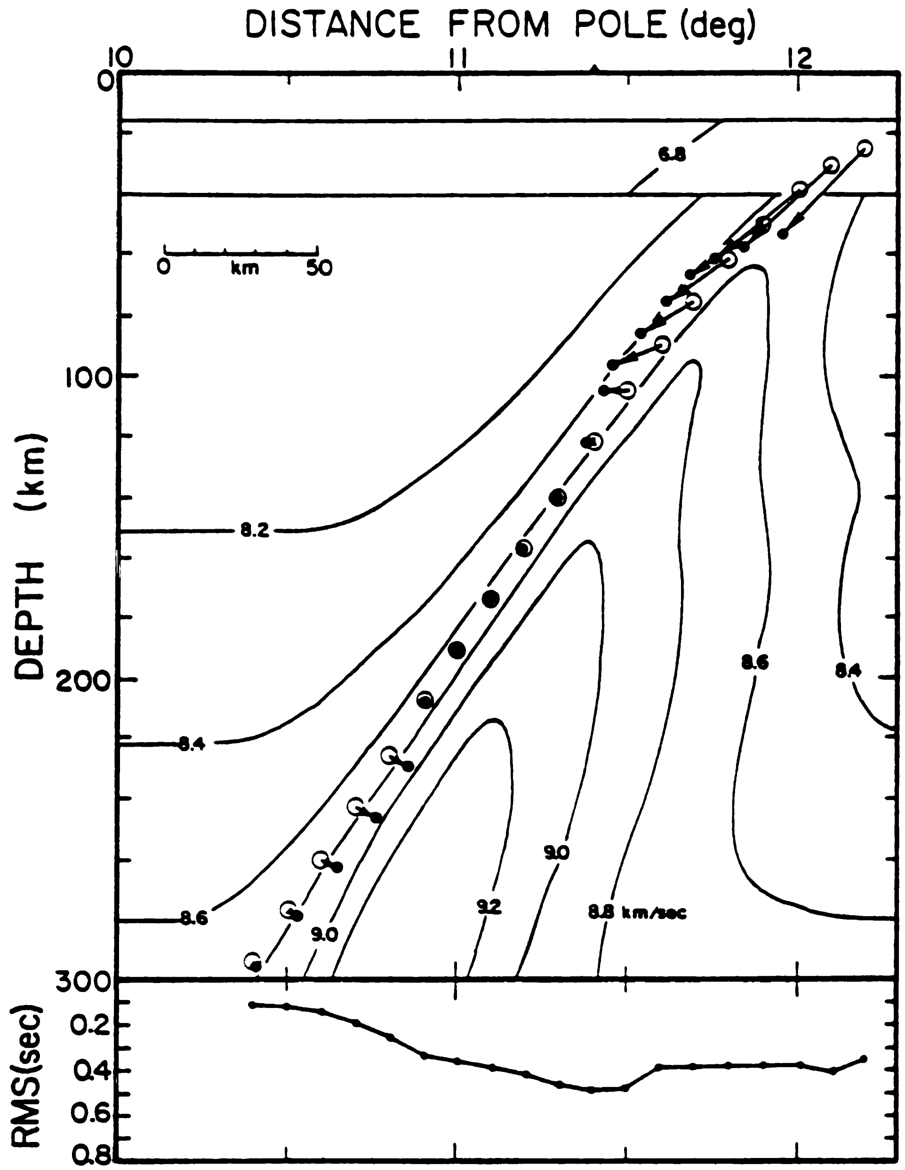


Figure 8. Deep Event Mislocation Vectors for 300 x 80 km, -.0009 Slab. Symbols same as in Figure 4. Relocations are done with large station set. Original hypothetical event locations (open circles) indicate the top surface of subducted slab.

events in subduction zones are probably more accurate than local network solutions even though they often show greater RMS residuals than the local solutions (Mclaren and Frohlich, 1985).

Also, note in Figure 8 the appearance of a spurious increase in slab dip at about 100 km depth resulting from the errant locations. This suggests that reported increases in the dip of actual Benioff zones at depth based on teleseismically determined locations may at least be partially the result of earthquake location errors. The mislocation vectors also show a subsequent decrease in dip at a depth of about 200 km, but this would probably not be seen since very little seismicity is recorded at this depth in the central Aleutians. It should be noted that a similar increase in dip at about 100 km depth has also been shown to appear as a result of slab induced location errors in local network solutions (Spencer and Engdahl, 1983; McLaren and Frohlich, 1985). Furthermore, the spurious increase in slab dip demonstrated for local network solutions is significantly greater than the effect determined here for teleseismic solutions.

Comparisons With Observed Seismicity

At this point I wish to determine if the model I have been using is a good match to the actual velocity structure in our study area. Before discussing the degree of fit to the model, evaluation of the actual mislocation data must be made to ensure that they are consistent. A major assumption in the modeling procedure is slab symmetry about a pole of rotation. If this assumption is a good approximation for the actual slab, then earthquakes along strike of the arc having the same $\partial$ value should show approximately the same degree of mislocation. Figure 9 shows mislocation vectors for the 40 events used in this study while Table 1 lists local and teleseismic locations for the events. As can be seen from Figure 9, mislocations for events between 175° and 176.2°W longitude (shown by an asterisk in Table 1) show significant variations for similar values of $\partial$. Topper (1978) suggested that a bend or tear exists in the slab at about 175.5°W with the slab to the east having a steeper and more northerly dip. The possible existence of considerable complexity in the slab in this area makes comparison with models assuming symmetry tenuous. Events between 176.2°W and 179°W (hereafter referred to as the "non-eastern" events) do, however, show a good deal of consistency with a few exceptions. Event # 19 (Table 1) did not converge upon relocation and was

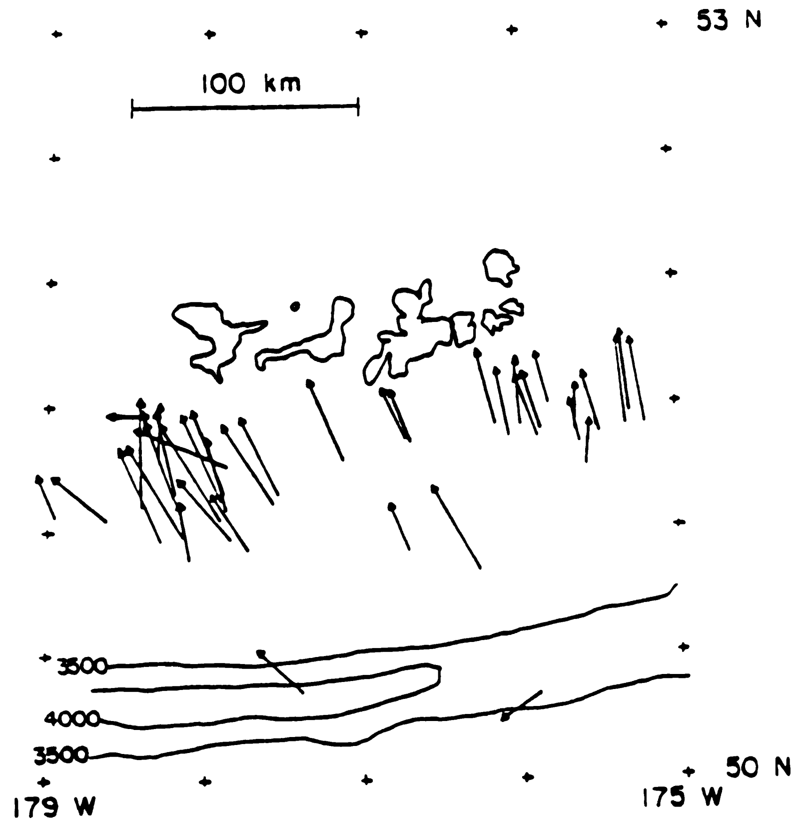


Figure 9. Mislocation Vectors for Actual Events. Epicentral mislocation vectors for the 40 events used in this study. Heads of arrows represent teleseismically determined locations, tails represent epicenters from the Adak local network. Bathymetric contours for the trench are given in meters. Adak and nearby islands are also shown.

Table 1. Teleseismic and Local Network Hypocenters of Actual Events. For each event, the first line gives the local network solution, the second line gives the teleseismic solution done with Herrin et al. (1968) travel times and Dziewonski and Anderson (1983) station corrections. *'s indicate eastern events; †'s indicate small non-eastern events; f's indicate depths fixed due to convergence above the surface.

| Date | hr | mn | sec | °lat(N) | °lon(W) | dp(km) | Mb | #obs. | res(sec) |
|---|---|---|---|---|---|---|---|---|---|
| 1. 74AUG13 | 03 | 46 | 19.78 | 51.147 | 177.880 | 14.7 | 5.7 | | |
| | | | 21.4 | 51.486 | 178.115 | 45.6 | 5.7 | 241 | .831 |
| 2. 74AUG14 | 05 | 34 | 53.31 | 51.118 | 177.904 | 12.9 | 5.6 | | |
| | | | 55.2 | 51.484 | 178.188 | 46.7 | 5.6 | 221 | .862 |
| 3. 74AUG16 | 09 | 41 | 31.03 | 51.113 | 177.555 | 15.0f | 5.6 | | |
| | | | 33.0 | 51.433 | 177.875 | 43.4 | 5.6 | 235 | .823 |
| 4.*74NOV28 | 05 | 28 | 46.18 | 51.420 | 175.189 | 11.4 | 5.1 | | |
| | | | 48.5 | 51.778 | 175.293 | 46.1 | 5.1 | 94 | .911 |
| 5.† 75JAN10 | 20 | 40 | 36.55 | 51.101 | 178.398 | 20.0f | 4.8 | | |
| | | | 39.4 | 51.536 | 178.432 | 42.3 | 4.8 | 48 | .720 |
| 6. 75JAN13 | 19 | 29 | 12.69 | 50.870 | 178.108 | 10.0f | 4.8 | | |
| | | | 15.3 | 51.098 | 178.224 | 24.0 | 4.8 | 62 | .687 |
| 7. 75MAR12 | 10 | 43 | 31.90 | 51.143 | 177.527 | 18.6 | 5.2 | | |
| | | | 33.7 | 51.459 | 177.778 | 39.8 | 5.2 | 133 | .733 |
| 8.*75MAR17 | 17 | 39 | 29.17 | 51.421 | 175.318 | 11.9 | 5.0 | | |
| | | | 31.4 | 51.789 | 175.384 | 50.5 | 5.0 | 100 | .706 |
| 9.*75MAR20 | 03 | 23 | 32.21 | 50.341 | 175.926 | 5.0f | 4.9 | | |
| | | | 33.0 | 50.233 | 176.095 | 10.0f | 4.9 | 91 | .918 |
| 10.†75APR02 | 14 | 43 | 20.26 | 51.279 | 178.296 | 20.0f | 4.8 | | |
| | | | 21.8 | 51.543 | 178.276 | 40.6 | 4.8 | 43 | .647 |
| 11. 75JUL08 | 20 | 57 | 21.21 | 51.147 | 178.213 | 16.9 | 4.8 | | |
| | | | 22.6 | 51.491 | 178.332 | 40.0 | 4.8 | 64 | .866 |
| 12.†76FEB18 | 08 | 00 | 58.8 | 51.466 | 178.381 | 13.8 | 5.0 | | |
| | | | 56.9 | 51.481 | 178.665 | 10.0f | 5.0 | 41 | .746 |
| 13.†76FEB22 | 07 | 2 | 24.52 | 51.315 | 176.629 | 25.0f | 5.0 | | |
| | | | 26.2 | 51.588 | 176.844 | 45.4 | 5.0 | 63 | 1.100 |
| 14.†76JUL22 | 14 | 30 | 14.49 | 51.085 | 177.870 | 16.3 | 4.9 | | |
| | | | 16.2 | 51.366 | 178.020 | 31.8 | 4.9 | 48 | .745 |
| 15. 76AUG16 | 05 | 11 | 37.00 | 51.140 | 178.233 | 17.5 | 5.2 | | |
| | | | 38.8 | 51.502 | 178.409 | 45.2 | 5.2 | 126 | .689 |
| 16.†76AUG28 | 17 | 29 | 27.80 | 50.923 | 177.753 | 15.0f | 5.0 | | |
| | | | 28.5 | 51.139 | 177.880 | 11.1 | 5.0 | 45 | .478 |
| 17.*76SEP22 | 02 | 30 | 25.80 | 51.401 | 175.857 | 20.6 | 4.8 | | |
| | | | 27.3 | 51.652 | 175.962 | 42.8 | 4.9 | 102 | .816 |
| 18.*77JAN06 | 16 | 02 | 06.72 | 51.255 | 175.556 | 11.2 | 5.3 | | |
| | | | 08.4 | 51.444 | 175.515 | 27.8 | 5.3 | 162 | .883 |
| 19. 77APR20 | 00 | 19 | 15.99 | 51.035 | 178.642 | 5.0f | 4.8 | | |
| (non-conv.) | | | 16.1 | 51.214 | 178.971 | 32.2 | 4.8 | 44 | .576 |
| 20.†77APR28 | 13 | 37 | 36.41 | 50.354 | 177.438 | 5.0f | 4.7 | | |
| | | | 38.1 | 50.516 | 177.713 | 10.0f | 4.7 | 47 | .985 |

Table 1 (cont'd.).

| Date | hr mn sec | °lat(N) | °lon(W) | dp(km) | Mb | #obs. | res(sec) |
|---|---|---|---|---|---|---|---|
| 21.*77JUN29 | 08 47 14.86 | 51.418 | 176.143 | 22.7 | 4.9 | | |
| | 16.7 | 51.744 | 176.256 | 51.6 | 4.9 | 108 | .780 |
| 22.*77AUG17 | 16 48 30.94 | 51.469 | 175.282 | 16.7 | 5.4 | | |
| | 33.0 | 51.817 | 175.362 | 55.3 | 5.4 | 162 | .830 |
| 23. 77SEP21 | 10 35 27.91 | 51.068 | 178.194 | 13.6 | 4.9 | | |
| | 30.0 | 51.461 | 178.367 | 38.9 | 4.9 | 98 | .889 |
| 24. 77OCT11 | 05 03 09.75 | 50.896 | 176.712 | 15.1 | 4.6 | | |
| | 12.8 | 51.112 | 176.883 | 27.8 | 4.6 | 82 | .659 |
| 25.*77NOV04 | 09 52 57.32 | 51.380 | 175.879 | 18.3 | 5.6 | | |
| | 59.7 | 51.642 | 176.024 | 50.6 | 5.6 | 268 | 1.080 |
| 26.*77NOV04 | 10 02 05.78 | 51.409 | 175.624 | 22.4 | 5.2 | | |
| | 06.6 | 51.607 | 175.619 | 38.9 | 5.2 | 86 | .692 |
| 27.*77NOV04 | 18 07 32.34 | 51.329 | 175.621 | 18.9 | 5.4 | | |
| | 34.2 | 51.518 | 175.680 | 40.8 | 5.4 | 204 | .985 |
| 28.*77NOV05 | 14 44 03.79 | 51.369 | 175.476 | 20.7 | 5.3 | | |
| | 06.6 | 51.584 | 175.664 | 46.5 | 5.3 | 230 | .990 |
| 29. 77DEC19 | 10 52 29.54 | 50.838 | 176.262 | 5.0f | 5.1 | | |
| | 38.6 | 51.152 | 176.529 | 34.8 | 5.1 | 143 | .707 |
| 30. 78JAN02 | 20 57 39.55 | 50.964 | 177.854 | 5.0f | 5.0 | | |
| | 39.9 | 51.200 | 178.209 | 28.6 | 5.0 | 134 | .684 |
| 31.*78JAN06 | 07 08 43.75 | 51.423 | 175.977 | 20.8 | 5.3 | | |
| | 44.6 | 51.710 | 176.016 | 52.7 | 5.3 | 144 | 1.030 |
| 32.*78APR24 | 04 28 47.37 | 51.354 | 176.057 | 10.0f | 5.2 | | |
| | 48.5 | 51.650 | 176.124 | 48.2 | 5.2 | 172 | .742 |
| 33.'78JUL21 | 20 50 29.72 | 51.038 | 177.904 | 5.0f | 4.9 | | |
| | 31.0 | 51.463 | 178.311 | 37.0 | 4.9 | 72 | .606 |
| 34.'78OCT17 | 20 50 48.22 | 51.358 | 176.723 | 25.0f | 4.9 | | |
| | 49.0 | 51.595 | 176.927 | 43.0 | 4.9 | 44 | .784 |
| 35.*79JAN31 | 03 07 32.22 | 51.513 | 175.793 | 25.0f | 5.1 | | |
| | 32.5 | 51.732 | 175.859 | 46.0 | 5.1 | 44 | .799 |
| 36. 79FEB12 | 05 11 06.88 | 51.058 | 178.943 | 5.0f | 4.7 | | |
| | 08.2 | 51.225 | 179.071 | 36.8 | 4.7 | 51 | .639 |
| 37.'82JAN04 | 23 37 35.05 | 51.249 | 177.869 | 11.3 | 4.8 | | |
| | 30.5 | 51.409 | 178.409 | 42.1 | 4.9 | 48 | .749 |
| 38. 82JUN04 | 03 01 03.88 | 51.282 | 177.094 | 21.4 | 5.7 | | |
| | 05.1 | 51.635 | 177.375 | 50.3 | 5.8 | 173 | .717 |
| 39. 82JUN15 | 19 57 36.91 | 50.976 | 178.156 | 1.0f | 5.0 | | |
| | 39.1 | 51.339 | 178.506 | 35.5 | 5.0 | 73 | .585 |
| 40.'83MAR22 | 01 32 29.79 | 50.952 | 178.278 | 6.8 | 4.9 | | |
| | 30.8 | 51.317 | 178.570 | 33.5 | 4.9 | 53 | .754 |

rejected. Event # 36 , at the far western edge of the study area, occurred at a time when the three westernmost stations of the Adak network were not operating and thus does not have a well constrained local solution.

Eleven of the smallest earthquakes (events 5,10,12,13,14,16,20,33,34, 37,40 in Table 1) were recorded by a distribution of teleseismic stations that is significantly different from the average station distribution for the rest of the events. Generally, mislocations for these events showed considerable scatter when compared to larger events having station geometries similar to those used to relocate the theoretical earthquakes. I suggest three possible reasons for this scatter.

1. Heterogeneities in the slab. This undoubtedly causes some scatter in mislocation effects, though it seems unlikely that this is the primary cause, since larger events do show a fair amount of consistency.

2. Errors in both local and teleseismic hypocentral determinations. The relatively small size of these events makes this a probable cause of a significant portion of the variation in mislocations.

3. Variations in station geometry used to locate these small events. Theoretical relocations indicate that station geometry variations will contribute somewhat to the scatter and make less reliable the comparisons with theoretical events located with the "average" station sets. Attempts

to make use of these smaller events will be discussed later.

After the foregoing analysis, I am left with 13 well located events recorded by a distribution of stations similar to the theoretical station sets. These are marked * in Table 1.

Mislocations for the "non-eastern" events (excluding those events with anomalous station geometries) were averaged for increments of 0.1° $\partial$ with a separation into large and small events depending on whether more or less than 175 stations reported the event. These averages, which are shown in Table 2, form the primary data set with which to compare model mislocations. It is obvious that this data set is rather limited both in quantity and spatial coverage with all of the events occurring in the thrust zone. The 6 events for a $\partial$ of 12.2° are quite consistent and constitute the statistically best set of data.

Since depths are much harder to constrain than epicenters, the primary emphasis in modeling will be on obtaining good agreement between epicentral mislocations. The evaluation procedure then, is to first evaluate the degree of fit of epicentral mislocations near 12.2° $\partial$ in the seismically active thrust zone, while looking secondarily at other thrust zone mislocations and at depth mislocations.

Table 2. Actual Event Mislocation Data.
Mislocations determined by comparing Adak local network solutions with teleseismic solutions computed with Herrin travel times and Dziewonski and Anderson (1983) station corrections (see text). Positive epicentral values indicate teleseismic mislocation to the north; positive depth values indicate teleseismic mislocation too deep. Right hand columns give averages of "large" and "small" events for each ∂; for 12.2° the standard deviation is also given.

| | | | | | Ave. misloc. for that ∂ (km) | | | |
|---|---|---|---|---|---|---|---|---|
| | Event # | | Mislocation (km) | | "large" | | "small" | |
| °∂ | (see Tab. 1) | # obs. | Epic. | Depth | Epic. | Depth | Epic. | Depth |
| 12.1 | 38 | 317 | 39.1 | 28.9 | 39.1 | 28.9 | | |
| 12.2 | 1 | 311 | 40.6 | 33.8 | 37.9 | 31.0 | 37.8 | 24.0 |
| | 2 | 365 | 37.6 | 30.9 | ±2.6 | ±2.7 | ±2.6 | ±3.3 |
| | 3 | 330 | 35.5 | 28.4 | | | | |
| | 7 | 171 | 35.0 | 21.2 | | | | |
| | 11 | 96 | 38.1 | 23.1 | | | | |
| | 15 | 174 | 40.2 | 27.7 | | | | |
| 12.3 | 23 | 136 | 43.7 | 25.3 | | | 43.7 | 25.3 |
| 12.4 | 30 | 175 | 26.2 | 23.6 | | | 33.3 | 29.1 |
| | 39 | 117 | 40.3 | 34.5 | | | | |
| 12.5 | 6 | 81 | 25.4 | 14.0 | 34.8 | 29.8 | | |
| | 24 | 105 | 23.9 | 12.7 | | | 24.7 | 13.4 |
| | 29 | 185 | 34.8 | 29.8 | | | | |

Comparison with the actual data set (see Tables 2 and 3) indicates that mislocations for the 300 x 80 km model with $\partial v/\partial T$ of $-9 \times 10^{-4}$ km/sec-°C are too small. Actual epicentral mislocations at 12.2° $\partial$ range from 35 to 40 km while the model predicts only 29 to 30 km of mislocation.

I suggest three possible reasons for the poor fit of this model. First, the poor agreement is due to incorrect position of the slab with respect to surface topography, which a study of amplitude anomalies on this identical model (Rogers, 1982) has indicated is plausible. This seems an unlikely explanation since the actual seismicity we have at 12.2° $\partial$ occurs where the model predicts the greatest mislocations. If the slab itself was significantly mislocated in the theoretical calculations, then the actual events now located at 12.2° would be located at a different $\partial$ where the model would predict even smaller mislocations. A second possibility for the poor fit is that the modeling technique used does not adequately represent the true velocity structure near Adak. It is, of course, difficult to assess the absolute reliability of the modeling routine given the inherent uncertainty of the nature of the slab/mantle interaction at depth. It should be noted, however, that thermally derived models have been used in numerous ray tracing studies (e.g. Jacob, 1972; Engdahl et al., 1977) to

Table 3. Theoretical Event Mislocation Data.
Theoretical mislocations for selected $\delta$'s for all models considered. Models are given by depth of penetration (km) by thickness (km), $\delta v/\delta T \times -10^{-4}$ km/sec-°C, and station set used for the relocations, s for small, l for large. Epicentral and depth mislocations are given in km, with positive epicentral values indicating teleseismic mislocation to the north and positive depth values indicating teleseismic depth mislocation too deep.

| | Mislocations (km) | | | | | | | | | | | | | | | |
|---|---|---|---|---|---|---|---|---|---|---|---|---|---|---|---|---|
| °δ→ | 11.6 | | 11.9 | | 12.1 | | 12.2 | | 12.3 | | 12.5 | | 12.8 | | 13.2 | |
| Model | Ep. | Dp. | Ep. | Dp. | Ep. | Dp. | Ep. | Dp. | Ep. | Dp. | Ep. | Dp. | Ep. | Dp. | Ep. | Dp. |
| 300x80,9 s | 1.3 | 13.5 | 19.6 | 17.8 | 28.4 | 19.3 | 30.0 | 19.2 | 31.1 | 17.0 | 29.7 | 12.7 | 19.7 | -2.8 | 6.0 | -20.6 |
| l | 9.7 | 9.1 | 24.0 | 14.2 | 28.9 | 16.4 | 29.0 | 16.6 | 28.4 | 14.7 | 24.6 | 10.0 | 14.7 | -8.6 | 4.7 | -23.8 |
| 300x80,11s | 2.2 | 16.3 | 22.6 | 22.1 | | | 35.3 | 24.8 | | | 35.9 | 17.9 | 26.5 | 5.7 | 10.5 | -20.3 |
| l | 12.0 | 10.9 | 28.5 | 17.5 | | | 34.8 | 21.1 | | | 30.6 | 14.4 | 20.7 | -0.3 | 7.4 | -15.0 |
| 300x100,9s | -0.8 | 14.0 | 17.6 | 18.4 | | | 29.9 | 20.6 | | | 29.5 | 14.7 | 22.3 | 3.6 | 10.3 | -18.4 |
| l | 8.3 | 9.5 | 23.1 | 14.5 | | | 29.5 | 18.0 | | | 25.4 | 11.7 | 17.6 | -0.7 | 7.4 | -15.0 |
| 360x80,5 s | | | | | | | 22.9 | 10.0 | | | | | | | | |
| l | | | | | | | 20.3 | 9.3 | | | | | | | | |
| 360x80,9 s | 10.2 | 16.4 | 27.6 | 21.6 | 36.9 | 24.0 | 39.2 | 23.7 | 39.3 | 21.8 | 36.9 | 16.9 | 27.0 | 4.7 | 10.7 | -21.0 |
| l | 17.4 | 12.4 | 31.0 | 18.2 | 36.1 | 21.2 | 36.5 | 21.3 | 35.2 | 19.1 | 30.7 | 14.0 | 20.5 | -2.2 | 7.6 | -15.0 |
| 360x80,11s | | | | | | | 44.7 | 30.2 | | | | | | | | |
| l | | | | | | | 43.1 | 26.3 | | | | | | | | |
| 360x100,5s | | | | | | | 22.6 | 11.2 | | | | | | | | |
| l | | | | | | | 20.9 | 10.2 | | | | | | | | |
| 360x100,9s | 6.8 | 17.9 | 25.9 | 22.9 | | | 37.5 | 25.3 | | | 37.8 | 19.8 | 30.1 | 10.9 | 15.9 | -10.9 |
| l | 15.9 | 12.7 | 30.6 | 18.5 | | | 36.5 | 22.0 | | | 32.2 | 16.4 | 23.5 | 4.5 | 11.4 | -21.0 |

Table 3 (cont'd.).

| | | Mislocations (km) | | | | | | | | | | | | | | | |
|---|---|---|---|---|---|---|---|---|---|---|---|---|---|---|---|---|---|
| | δ→ | 11.6 | | 11.9 | | 12.1 | | 12.2 | | 12.3 | | 12.5 | | 12.8 | | 13.2 | |
| Model | | Ep. | Dp. | Ep. | Dp. | Ep. | Dp. | Ep. | Dp. | Ep. | Dp. | Ep. | Dp. | Ep. | Dp. | Ep. | Dp. |
| 420x80,7 | s | | | 28.9 | 18.4 | | | 37.7 | 19.9 | | | 34.3 | 14.6 | | | | |
| | 1 | | | 30.5 | 16.5 | | | 33.9 | 18.4 | | | 27.8 | 12.2 | | | | |
| 420x80,8 | s | | | 32.5 | 21.5 | | | 42.2 | 23.6 | | | 40.0 | 18.5 | | | | |
| | 1 | | | 34.3 | 18.9 | | | 38.4 | 21.5 | | | 32.9 | 15.9 | | | | |
| 420x80,9 | s | 16.5 | 18.6 | 35.4 | 24.5 | | | 46.4 | 27.4 | | | 44.8 | 21.9 | 34.9 | 12.5 | 17.6 | -11.6 |
| | 1 | 23.6 | 13.9 | 38.0 | 21.0 | | | 42.8 | 24.8 | | | 37.2 | 18.8 | 26.9 | 5.2 | 12.5 | -24.2 |
| 480x80,7 | s | | | 34.5 | 20.4 | | | 43.3 | 22.7 | | | 40.0 | 18.0 | | | | |
| | 1 | | | 35.1 | 18.8 | | | 38.5 | 21.6 | | | 32.5 | 15.9 | | | | |
| 540x80,5 | s | | | | | | | 34.9 | 16.2 | | | | | | | | |
| | 1 | | | | | | | 30.0 | 15.9 | | | | | | | | |
| 540x80,6 | s | | | 34.8 | 19.0 | | | 42.3 | 20.9 | 41.3 | 19.5 | 37.7 | 16.8 | 28.1 | 7.2 | 13.4 | -15.3 |
| | 1 | | | 34.4 | 18.5 | | | 37.9 | 20.7 | 35.1 | 19.0 | 30.2 | 15.1 | 21.2 | 1.3 | 9.5 | -15.0 |
| 540x80,7 | s | | | 39.4 | 22.3 | | | | | | | | | | | | |
| | 1 | | | 39.5 | 21.1 | | | | | | | | | | | | |

successfully demonstrate various slab effects. One area where the models used in this study are likely in error is the leading edge of the downgoing slab, which I have represented as having a rectangular shape. More realistic models assume the leading edge to be tapered or rounded in shape. However, since so few rays actually exit at the bottom of the slab, this discrepency will have negligible effect on the results. Assuming, then, that the modeling technique is essentially reliable, I suggest that the poor mislocation agreement is due to the inadequacy of this particular model. Therefore, I need to adjust the model parameters in order to increase mislocations.

One way to increase travel time residuals, and hence mislocations, is to simply increase $\partial v/\partial T$, thereby increasing the velocity contrast for the same size model. Analysis of a 300 x 80 km slab model with a $\partial v/\partial T$ of $-11 \times 10^{-4}$ km/sec-°C shows that this does indeed increase mislocations, though the mislocations are still slightly too small (see Tables 2 and 3). A 300 x 80 km slab with a $\partial v/\partial T$ slightly larger than $-11 \times 10^{-4}$ would likely result in a good fit with the data. However, the model with a $\partial v/\partial T$ of $-11 \times 10^{-4}$ gives an average velocity contrast of ~8% and a maximum velocity contrast of ~12% (Figure 10), values which are probably unreasonably high (Utsu, 1971; Hasegawa et al., 1978; Suyehiro and Sacks, 1979). Such

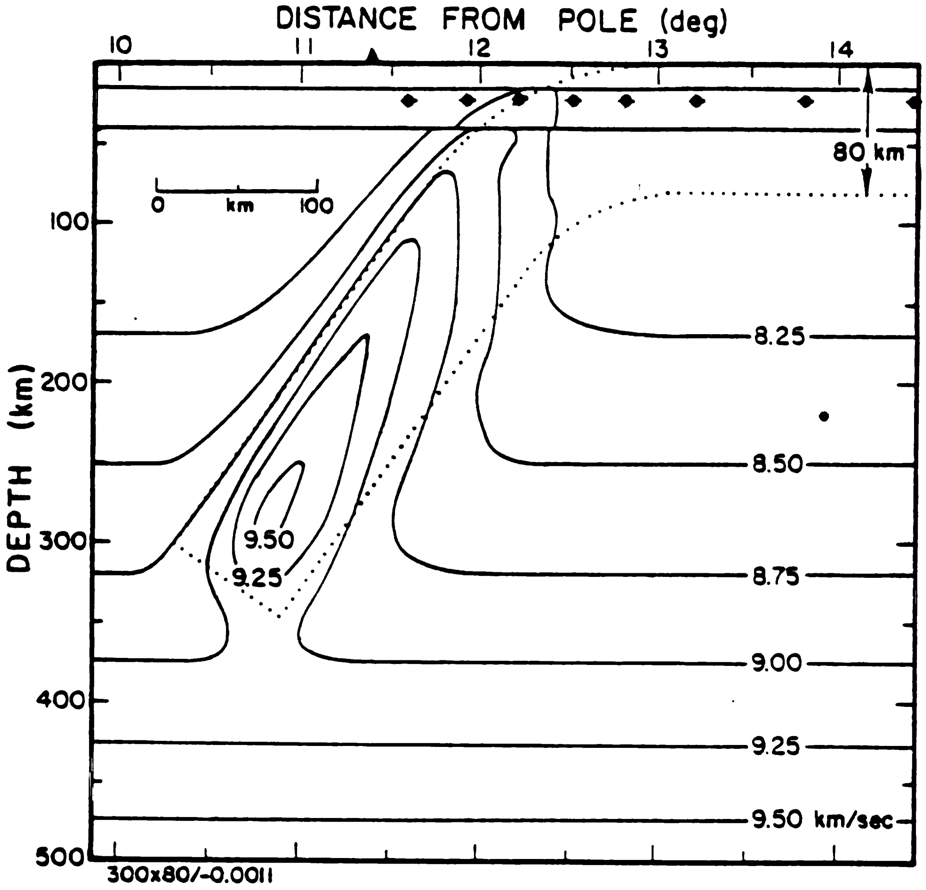


Figure 10. Velocity Profile of 300 x 80, -.0011 Slab. Symbols same as in Figure 2.

contrasts would result in very pronounced shadow zones, the degree of which have not been observed (Sleep, 1973; Rogers, 1982). Therefore, a 300 by 80 km slab with such a high velocity contrast does not appear to be a reasonable model. Such a model also makes ray tracing into these shadow zones very difficult, with increments in takeoff angle as small as .0001° resulting in differences of greater than 10° geocentric distance upon emergence at the surface.

Another possible way to increase travel time advances is to increase the size of the slab. First, I attempt to improve the fit by increasing the thickness from 80 to 100 km, while keeping the depth at 300 km and the thermal coefficient at $-9 \times 10^{-4}$ km/sec-°C. Examination of the resulting velocity profile (Figure 11) shows that this increases the overall velocity contrast with the adjacent mantle very little; it merely has the effect of widening the zone of anomalous velocity. Also seen is that increasing the thickness affects the degree of mislocation significantly only in the forearc and outer rise regions, with little difference in the thrust zone (see Table 3). Similar results are obtained by comparing 360 x 80 km and 360 x 100 km models. Mislocations at $\partial$'s of 12.8° and 13.2° are affected by 3 to 4 km in epicenter and up to 10 km in depth. Since I have little or no actual data outside the thrust zone, I cannot confidently constrain the

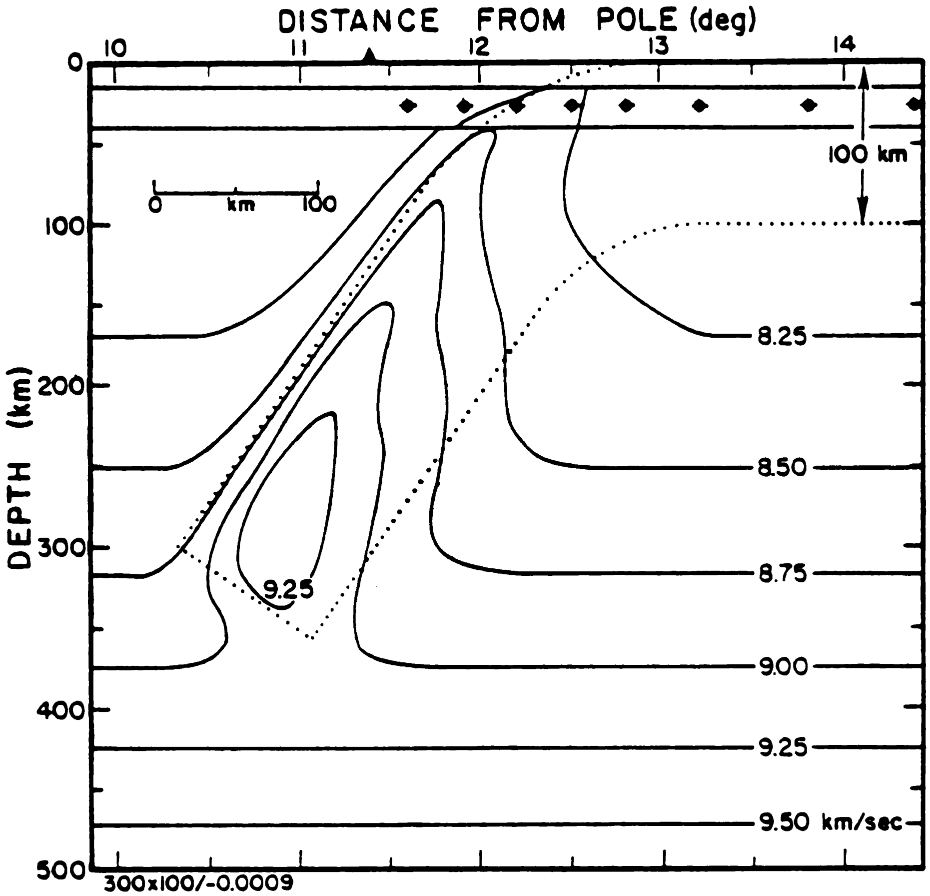


Figure 11. Velocity Profile of 300 x 100, -.0009 Slab. Symbols same as in Figure 2.

thickness of the slab in this study. Therefore, I assume a thickness of 80 km in all subsequent models since this agrees roughly with the predicted values based on flexural studies (Watts and Talwani, 1974) and age considerations (Yoshii et al., 1976).

The other alternative is to increase the length of the downgoing slab. Examination of model mislocations for a 360 km deep by 80 km thick slab with a $\partial v/\partial T$ of $-9 \times 10^{-4}$ shows good agreement with the actual data set. At 12.2° ∂, the model predicts epicentral mislocations of 39.2 and 36.5 km for the small and large station sets, respectively, while the data set gives average epicentral mislocations of 37.8 and 37.9 km for "small" and "large" events, respectively. Subsequent increases in depth with corresponding decreases in the thermal coefficient give models with similar mislocations in the thrust zone. (refer to Figures 12 and 13 and Table 3). For a depth of 420 km, the best fit model would have a thermal coefficient between $-7 \times 10^{-4}$ and $-8 \times 10^{-4}$ °C-km/sec. For a depth of 480 km, the thermal coefficient would be somewhat less than $-7 \times 10^{4}$; for 540 km, $\partial v/\partial T$ would be between $-5 \times 10^{-4}$ and $-6 \times 10^{-4}$.

The rest of the thrust zone data shows more scatter. The one "large" earthquake at 12.1° ∂ has an epicentral mislocation of 39.1 km which would require a slightly longer slab and/or higher thermal coefficient than the

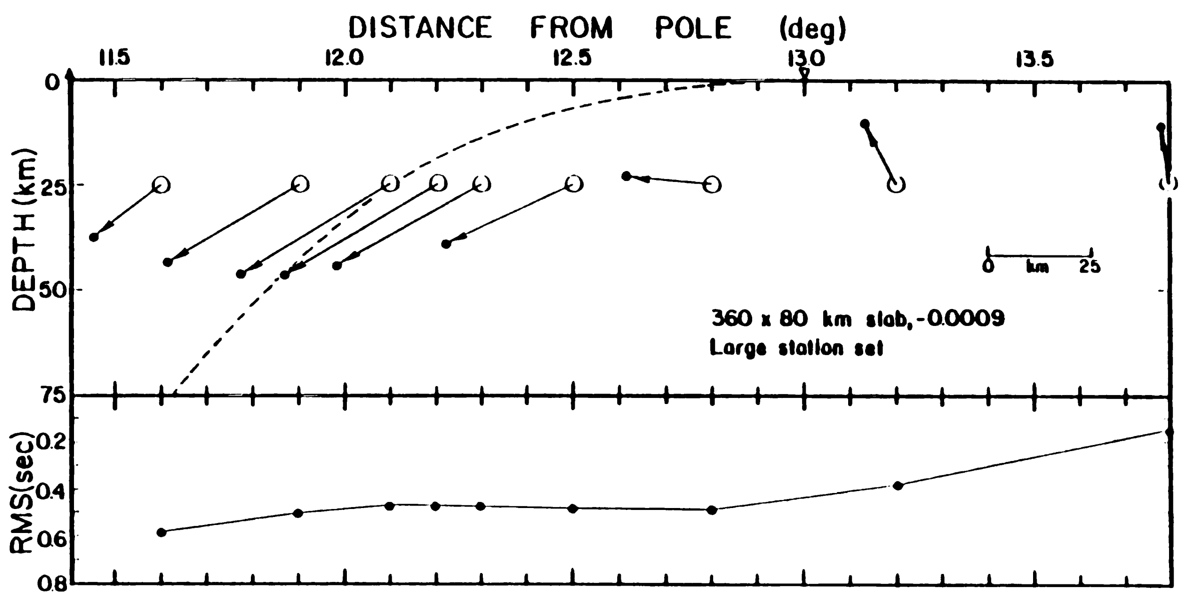


Figure 12. Shallow Event Mislocation Vectors for 360 x 80, -.0009 Slab. Symbols same as in Figure 4. Relocations shown are done with large station set.

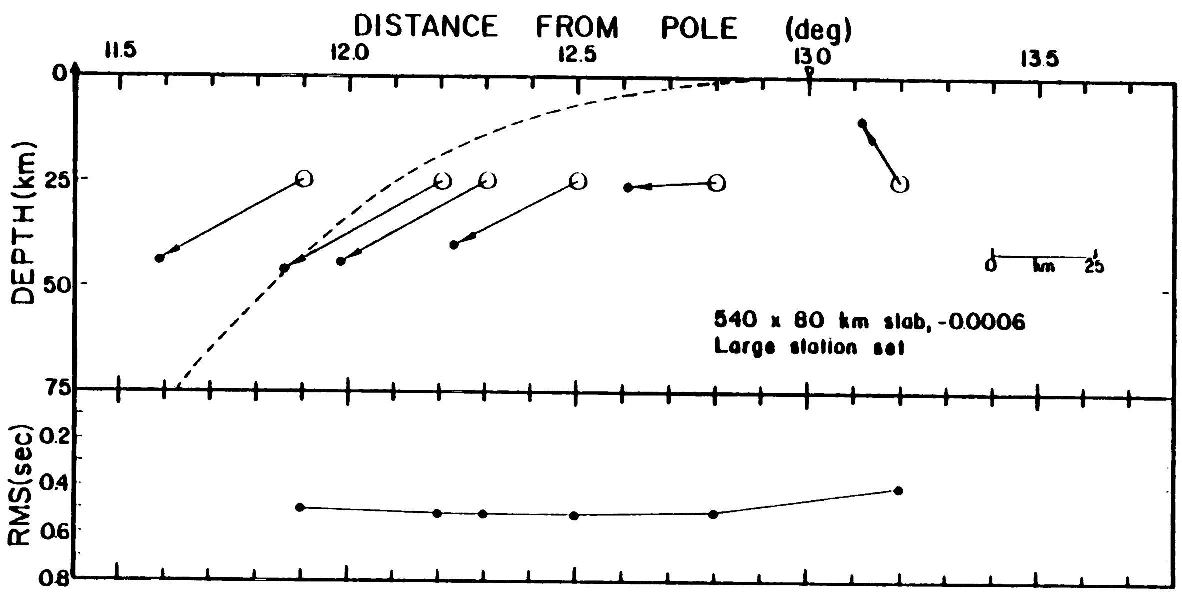


Figure 13. Shallow Event Mislocation Vectors for 540 x 80, -.0006 Slab. Symbols same as in Figure 4. Relocations shown are done with large station set.

above results indicate. The same is true of the one "small" event at 12.3° ∂ (epicentral mislocation of 43.7), the "small" event at 12.4° ∂ (40.3 km), and the "large" event at 12.5° ∂ (34.8 km). The "small" event at 12.4° ∂ (epicentral mislocation of 26.2 km) and the two "small" events at 12.5° ∂ (25.4 and 23.9 km) argue for a shorter slab and/or a smaller $\partial v/\partial T$.

Depth mislocations for actual events are generally greater than for model events. Model depth mislocations can be increased by up to 10 km if the travel time to ADK is determined using a standard Herrin travel-time table rather than the table modified to include shallow structure under ADK. Using a J-B travel-time table (Jeffreys and Bullen, 1940) results in a further increase in model depth mislocations of 1 or 2 km. Hence, improved agreement with actual depth mislocations is obtainable by simply changing the travel-time table used. Therefore, due to the variability in depth locations, I do not attempt any conclusions based on depths.

An attempt was made to utilize several smaller events having anomalous station geometries. Theoretical event relocations corresponding to the location of the actual event were made for several of the "favored" models using the identical station set used to locate the actual earthquake. In general, this did not decrease the scatter or improve the fit to the "favored" models for these events. Thus, the variation in mislocations for these smaller events does not appear to be primarily caused by station geometry differences. Likely, the scatter is predominantly due to uncertainties in the locations for events of this small size.

There appears to be, in general, an approximately linear relationship between depth and thermal coefficient in the model mislocations. The maximum reasonable depth of the slab, assuming experimental values for $\partial v/\partial T$ of $-5 \times 10^{-4}$ km/sec-°C, would likely occur at a depth slightly less than 600 km. Comparison with the data, then, gives us a range of feasible models from 360 km depth and a $\partial v/\partial T$ of $-9 \times 10^{-4}$ to about 600 km with a $\partial v/\partial T$ of $-5 \times 10^{-4}$ km/sec-°C.

## DISCUSSION

Given the limited set of earthquakes with which to compare the modeling data, I cannot easily differentiate at this time between the range of best fit models given above based on the observed seismicity for the central Aleutian slab. However, theoretical results indicate that, if a more complete set of data were available, better constraints are possible. One possible discriminator between models, especially for thickness, is the variation of mislocations with varying $\partial$. Some models show similar mislocations in the thrust zone while having somewhat different mislocations outside the thrust zone; for example compare models 300x80,9 to 300x100,9,and 360x80,9 to 360x100,9, at $\partial = 13.2°$ in Table 3. At this location, better constraints on local network solutions would have to be obtained to make reliable comparisons. The additional deployment of ocean bottom seismographs would be very helpful (Frohlich et al., 1982). Better depth constraints, perhaps through the use of depth phases, could be very useful given the relatively large differences in depth mislocations.

Another potential discriminator is the comparison of different size earthquakes occurring in the same vicinity in the thrust zone. Modeling results show that different size events occurring in the same place can be teleseismically located differently as a result of station geometry differences (see Table 3). For model thrust zone events, comparison of epicentral mislocations for the two model station sets reveals distinct patterns. For a ∂ of 11.9°, shorter slab models (300 x 80 with $\partial v/\partial T$ of $-9 \times 10^{-4}$ and $-11 \times 10^{-4}$ km/sec-°C and 360 x80 with $\partial v/\partial T$ of $-9 \times 10^{-4}$ km/sec-°C) show mislocation differences between the two station sets of 3.5 to 6 km while reasonable, longer models (480 and 540 km depth of penetration) have differences of less than 1 km. For 12.2° ∂, the opposite pattern emerges. Shorter slabs show small differences (1 or 2 km) while longer slabs show greater differences (4 or 5 km). At 12.5° ∂, the effects are less dramatic, with shorter slabs showing smaller differences (5 or 6 km) than longer slabs (7.5 km). A large number of events would be required to make a statistically significant comparison, since differences are on the order of a few kilometers. I can cautiously apply the above criteria to the data. Note that in the limited set of events at 12.2° ∂, there doesn't appear to be a clear relationship between the degree of mislocation and the number of stations reporting the event. For the six actual events occurring near 12.2° ∂, the average epicentral mislocation is almost identical for the 3 "large" events and the 3 "small" events. Although this is a rather limited number of events, the lack of variation in mislocation with event size favors the shorter slab models.

For the determined range of best fit models, my feeling is that the 360 km depth of penetration is most realistic for several reasons. First, the foregoing discussion of station sets tenuously favors a shorter slab model. Second, a depth of 360 km agrees roughly with the 386 km best fit depth determined by Spencer and Engdahl (1983) using velocity inversion. Third, depths much greater than 360 km would be difficult to explain based on assumed plate velocities and the estimated time since subduction originated (Hays and Ninkovich, 1970; Sleep, 1973).

The deepest recorded seismicity in the region of this study is at approximately 260 km depth. This study suggests that the slab penetrates at least 100 km beyond this point, supporting recent studies that indicate subducting lithosphere can retain its anomalous character in the mantle far beyond the point of detectable seismicity (e.g. Jordan, 1977; Creager and Jordan, 1984). To my knowledge, the largest previous estimate for the depth of penetration of the central Aleutian slab is the 386 km estimate of Spencer and Engdahl (1983). The results presented here indicate that the slab could conceivably penetrate as much as 200 km beyond this previous maximum, though I feel this is unlikely.

If the 360 x 80 km model ($\partial v/\partial T$ = -9 x $10^{-4}$ km/sec-°C) is grossly correct, then an estimate of the temperature at which the deepest observed seismicity occurs can be made for the slab near Adak. Molnar et al. (1979) examined the depths of deepest observed seismicity in numerous subduction zones to derive a relationship between cut-off temperatures for seismicity and depth. Their results predict a cut-off temperature of 630 ± 100°C for a depth of 260 km. The temperature profile for the preferred model here, however, gives a coldest temperature of about 800°C at 260 km depth. Temperatures as cold as those predicted by Molnar et al. (1979) would not occur at this depth using my modeling procedure unless the slab was extremely fast and/or thick. It is likely that the close proximity of the Adak local network allows detection of smaller events occurring at greater temperatures than those determined by Molnar et al. (1979) for a given depth.

Using the 360 x 80 km ($\partial v/\partial T$ = -9 x $10^{-4}$ km/sec-°C) slab as the preferred model, I then performed theoretical relocations for two parallel sets of intermediate depth events intended to represent a Benioff double seismic zone. One set of events was located along the upper surface of the descending slab, while the other set was within the slab 31 km from the upper surface. Figure 14 shows the mislocation vectors and indicates that

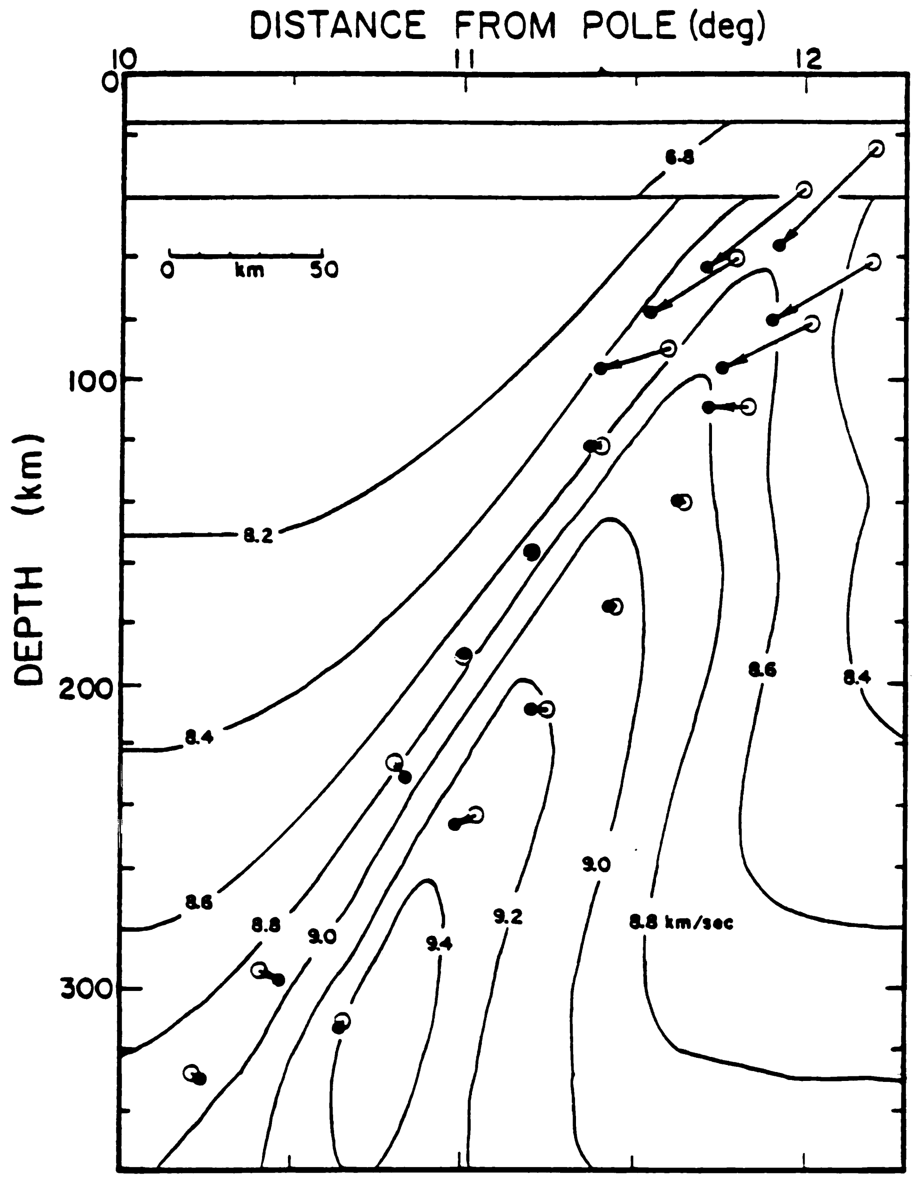


Figure 14. Deep Event Mislocation Vectors for 360 x 80 km, -.0009 Slab. Symbols same as in Figure 4.

the two major conclusions from intermediate depth mislocations in the original 300 km deep model are unchanged; events below about 100 km depth are mislocated by less than 10 km in epicenter and the mislocations give rise to a spurious increase in slab dip at about 100 km depth. Note also that below about 200 km depth, the mislocations cause the 31 km separation of the double seismic zone to appear narrower than it actually is. The pair of events near 240 km depth appear to be only 22 km apart upon teleseismic relocation. This implies that estimates of the thickness of Benioff zones may be too small at certain depths when based on teleseismically determined hypocenter distributions. The teleseismic mislocations of these events are not great enough, however, to entirely account for the eventual merging of the double zone into a single seismic zone, which has been reported to occur at approximately 175 km depth in the Japan, Kurile and Kamchatka arcs (Fujita and Kanamori, 1981).

# CONCLUSIONS

In this study, I have attempted to use thermal modeling, along with seismic ray tracing, to delineate the gross velocity structure of a subduction zone. The way in which the higher velocity slab affects compressional wave travel times, and thus, earthquake locations, forms the basis for the modeling procedure. Published hypocenters for island arc earthquakes located using teleseismic arrivals and standard location routines can be in error by more than 50 km (Engdahl, 1977). The degree of teleseismic mislocation is estimated by comparing ISC and PDE reported hypocenters with hypocenters determined from local network data only. Local networks give accurate solutions for events relatively close to the land based network, primarily thrust zone events (Frohlich et al., 1982), while more distant earthquakes in the forearc and outer rise are less reliably located by the local network.

Modeling results indicate that teleseismic locations of island arc earthquakes can be grossly in error when location routines assuming a spherically symmetric earth are used. The greatest mislocations occur in the shallow thrust zone, the amount depending on the specific characteristics of the slab. Changes in the depth of penetration of the slab and the assumed thermal coefficient have pronounced effects on model mislocations, while variations in slab thickness result in only minor variations to velocity profiles and model mislocations.

From comparison with actual earthquakes occurring in the central Aleutians, the results suggest that the subducting slab in this region penetrates to a depth well in excess of 300 km but probably not deeper than 600 km assuming that the thermal coefficient varies between $-5 \times 10^{-4}$ and $-9 \times 10^{-4}$ km/sec-°C. The smaller value is constrained by laboratory experiments (Anderson, 1968), while the larger value is constrained on the basis of previous studies (e.g. Sleep, 1973), and velocity contrast and shadow zone considerations. Within the range of models suggested by comparison with observed seismicity, the preferred model has a thickness of 80 km, a depth of penetration of 360 km, and a thermal coefficient of $-9 \times 10^{-4}$ km/sec-°C based on agreement with the results of Spencer and Engdahl (1983) and on estimates of the duration of subduction and plate velocities for the central Aleutians (Hays and Ninkovich, 1970).

Theoretical results suggest that models could be further constrained given a more complete set of seismicity data in the area. Variations in mislocations with changing $\partial$ exist for models having similar mislocations in the seismically active thrust zone. Data in the forearc and outer rise would be especially helpful in constraining thickness. Also, a larger number of events in the thrust zone could be used to determine mislocation differences for various size earthquakes. Theoretical results indicate that such differences resulting from variations in station geometry could be used to differentiate between models if a statistically significant number of events were available. The limited data set used in this study favors the shorter slab models (i.e. 360 km depth of penetration) based on this reasoning.

My results, then, suggest a depth of slab penetration of about 100 km, and perhaps several hundred km, deeper than the deepest recorded seismicity in the area of study (260 km). This supports the theory that slabs can retain their anomalous velocity characteristics well beyond the point where they cease to generate detectable seismicity.

Modeling of deeper focus events occurring along the upper surface of the slab suggest that events deeper than about 100 km are probably not significantly mislocated teleseismically. Teleseismic mislocations may also be at least partly responsible for reported increases in both the dip of the Benioff zone at depth and the merging of the double zone into a single seismic zone.

The modeling routine used here suffers from several limitations. The thermally derived velocity profile representing the subducting slab is necessarily simplified. While thermal modeling, in theory, can be made as complex as one wishes, the added uncertainty involved with very detailed structures precludes their usefulness given the present understanding of subduction zones. The thermal modeling technique requires numerous assumptions while the ray tracing technique is approximate.

Other possible sources of uncertainty include plotting and digitizing errors, representation of residuals by a finite number of Fourier coefficients, and minor variations in station sets used. In most cases, these errors are minor, and improvements are not warranted given the degree of uncertainty in earthquake location routines.

# BIBLIOGRAPHY

# BIBLIOGRAPHY

Anderson, O.L., Schreiber, E., and Liebermann, R.C., 1968. Some elastic constant data on minerals relevant to geophysics. Rev. Geophys., 6: 491-524.

Barazangi, M., and Isacks, B.L., 1979. A comparison of the spatial distribution of mantle earthquakes determined from data provided by local and by teleseismic networks for the Japan and Aleutian arcs. Bull. Seismol. Soc. Am., 69: 1763-1770.

Creager, K.C., and Jordan, T.H., 1984. Slab penetration into the lower mantle, J. Geophys. Res., 89: 3031-3049.

Dziewonski, A.M., and Anderson, D.L., 1983. Travel times and station corrections for P waves at teleseismic distances. J. Geophys. Res., 88: 3295-3314.

Engdahl, E.R., 1977. Seismicity and plate structure in the central Aleutians. In: Talwani, M., and Pitman, W.C. III (eds.), Island Arcs, Deep Sea Trenches and Back-Arc Basins. Am. Geophys. Union, Washington, D.C., 259-271.

Engdahl, E.R., Kisslinger, C., LaForge, R.C., Price, S., Topper, R., and Johnston, A.C., 1977a. A field study of earthquake prediction methods in the central Aleutian Islands. Semi-annual tech. report, 1 Oct., 1976- 31 Mar., 1977, U.S. Geol. Survey.

Engdahl, E.R., Sleep, N.H., and Lin, M.-T., 1977b. Plate effects in North Pacific subduction zones. Tectonophysics, 37: 95-116.

Engdahl, E.R., Dewey, J.W., and Fujita, K., 1982. Earthquake location in island arcs. Phys. Earth Planet. Inter., 30: 145-156.

Frohlich, C., Billington, S., Engdahl, E.R., and Malahoff, A., 1982. Detection and location of earthquakes in the central Aleutian subduction zone using island and ocean bottom seismograph stations. J. Geophys. Res., 87: 6853-6864.

Fujita, K., Engdahl, E.R., and Sleep, N.H., 1981. Subduction zone calibration and teleseismic relocation of thrust zone events in the central Aleutian Islands. Bull. Seismol. Soc. Am., 71: 1805-1828.

Fujita, K., and Kanamori, H., 1981. Double seismic zones and stresses of intermediate depth earthquakes. Geophys. J.R. Astron. Soc., 66: 131 - 156.

Hasegawa, A., Umino, N., and Takagi, A., 1978. Double-planed deep seismic zone and upper-mantle structure in the Northeastern Japan Arc. Geophys. J.R. Astron. Soc., 54: 281-296.

Hays, J., and Ninkovich, D., 1970. North Pacific deep sea ash chronology and age of present Aleutian underthrusting. Geol. Soc. Am. Mem. 126: 263-290.

Herrin, E., and Taggart, J., 1968. Regional variations in P travel times. Bull. Seismol. Soc. Am., 58: 1325-1337.

Herrin, E., Arnold, E.P., Bolt, B.A., Clawson, G.E., Engdahl, E.R., Freedman, H.W., Gordon, D.W., Hales, A.L., Lobdell, J.L., Nuttli, O., Romney, C., Taggart, J., and Tucker, W., 1968. 1968 Seismological tables for P phases. Bull. Seismol. Soc. Am., 58: 1196-1241.

Jacob, K., 1970. Three-dimensional seismic ray tracing in a laterally homogeneous spherical earth. J. Geophys. Res., 75: 6675-6689.

Jacob, K., 1972. Global tectonic implications of anomalous P travel-times from the nuclear explosion Longshot. J. Geophys. Res., 77: 2556-2573.

Jeffreys, H. and Bullen, K.E., 1940. Seismological Tables, Brit. Assn., London, 1940.

Jordan, T.H., 1977. Lithospheric slab penetration into the lower mantle beneath the Sea of Okhotsk. J. Geophys., 43: 473-496.

Kisslinger, C., Billington, S., Bowman, R., Cruz, G., Huang, Z.-X., Pohlman, J., Toth, T., and Morrissey, S.-T., 1982. A field study of earthquake prediction methods in the central Aleutian Islands. Semi-annual tech. report, Sep. 30, 1982, U.S. Geol. Survey.

Kisslinger, C., Billington, S., Silliman, A., McDonald, C., Toth, T., Perin, B., Harjes, M., and Morrissey, S.-T., 1984. A field study of earthquake prediction methods in the central Aleutian Islands. Final Tech. Report, Jan. 30, 1984, U.S. Geol. Survey.

Mclaren, J.P., and Frohlich, C., 1985. Model calculations of regional network locations for earthquakes in subduction zones. Bull. Seismol. Soc. Am., 75: 397-413.

Molnar, P., Freedman, D., and Shih, J.S.F., 1979. Lengths of intermediate and deep seismic zones and temperatures in downgoing slabs of lithosphere. Geophys. J.R. Astron. Soc., 56: 41-54.

Rogers, W.J.,Jr., 1982. The effects of subducting slabs on seismic amplitudes and travel-times from forearc and outer rise earthquakes. M.S. Thesis, Michigan State University, East Lansing, MI.

Sleep, N.H., 1973. Teleseismic P-wave transmission through slabs. Bull. Seismol. Soc. Am., 63: 1349-1373.

Spencer, C.P., and Engdahl, E.R., 1983. A joint hypocentre location and velocity inversion technique applied to the Central Aleutians. Geophys. J.R. Astron. Soc., 72: 399-415.

Suyehiro, K., and Sacks, I.S., 1979. P- and S-wave velocity anomalies associated with the subducting lithosphere determined from travel-time residuals in the Japan region. Bull. Seismol. Soc. Am., 69: 97-114.

Toksoz, M.N., Minear, J.W., and Julian, B.R., 1971. Temperature field and geophysical effects of a downgoing slab. J. Geophys. Res., 76: 1113 - 1138.

Toksoz, M.N., Sleep, N.H., and Smith, A.T., 1973. Evolution of the downgoing lithosphere and the mechanism of deep focus earthquakes. Geophys. J.R. Astron. Soc., 35: 285-310.

Topper, R.E., 1978. Fine structure of the Benioff zone beneath the central Aleutian arc. M.S. Thesis, University of Colorado, Boulder, CO.

Toth, T., and Kisslinger, C., 1984. Revised focal depths and velocity model for local earthquakes in the Adak seismic zone. Bull. Seismol. Soc. Am., 74: 1349-1360.

Utsu, T., 1971. Seismological evidence for anomalous structure of island arcs with special reference to the Japanese region. Rev. Geophys. Space Phys., 9: 839-890.

Watts, A.B., and Talwani, M., 1974. Gravity anomalies seaward of deep-sea trenches and their tectonic implications. Geophys. J.R. Astron. Soc., 36: 57-90.

Yoshii, T., Kono, Y., and Ito, K., 1976. Thickness of the oceanic lithosphere. In: Sutton, G.N., Manghanani, M.H., Moberly, R., and McAffe, E.V. (eds.), The Geophysics of the Pacific Ocean Basin and its Margins. Geophys. Monogr., A. G. U., 19: 423-430.